



ARTICLE

Synthesis, crystal structure elucidation, DFT analysis, drug-likeness and ADMET evaluation and molecular docking studies of triazole derivatives: Binary inhibition of spike protein and ACE2 receptor protein of COVID-19

Saminathan Murugavel¹  | Perumal Vasudevan¹ |
 RaviKumar Chandrasekaran²  | Vellingiri Archana³ |
 Alagusundaram Ponnuswamy⁴

¹Department of Physics, Thanthai Periyar Government Institute of Technology, Vellore, Tamil Nadu, India

²Department of Physics, Thanthai Periyar EVR Government Polytechnic College, Vellore, Tamil Nadu, India

³Department of Chemistry, School of Physical Sciences and Computational Sciences, Avinashilingam Institute for Home Science and Higher Education for Women, Coimbatore, Tamil Nadu, India

⁴Department of Organic chemistry, School of chemistry, Madurai Kamaraj University, Madurai, Tamil Nadu, India

Correspondence

Saminathan Murugavel, Department of Physics, Thanthai Periyar Government Institute of Technology, Vellore, Tamil Nadu 632002, India.
 Email: smurugavel27@gmail.com

Funding information

Tamil Nadu State Council for Science and Technology, DOTE Campus, Chennai, Tamil Nadu, India, Grant/Award Number: TNSCST/STP/PS-03/2019-20/3680

Abstract

The recent incidence of terrible acute respiratory syndrome coronavirus 2 (SARS CoV-2) has presently experienced some noteworthy mutations since its discovery in 2019 in Wuhan, China. The present research work focuses on the synthesis of three triazole derivatives (BMTTP, BMTTP, and BMTIP) and their inhibition activities against SARS-Cov-2 spike and ACE2 receptor proteins. The crystal structure for BMTTP was determined by the SCXRD method and optimized geometrical parameters for the three triazole derivatives were obtained by DFT calculations. HOMO-LUMO, Global reactive descriptors [GRD], and Molecular electrostatic potential (MEP) investigations exposed that all three compounds have biological properties. The drug-likeness ability of the synthesized compounds was examined using Molinspiration and a pre-ADMET online Server. Further, to explore the binding nature of three synthesized compounds with SARS-Cov-2 spike proteins/ACE2 receptor molecular docking studies were executed. The outcomes we obtained from molecular docking simulation studies suggest that the synthesized triazole derivatives may be well utilized as curing medicines against COVID-19. Ultimately, animal tests and precise clinical tests are required to prove the potent nature of these compounds against COVID-19. Finally, the present outcomes must be proved to utilize in-vitro and in-vivo antiviral methods.

KEYWORDS

ADMET, COVID-19, crystal structure, DFT, docking, drug-likeness, triazole

1 | INTRODUCTION

The recent happening of severe acute respiratory syndrome coronavirus 2 (SARS CoV-2) has currently experienced several noteworthy mutations since its discovery in 2019 in Wuhan, China. The Beta variant, Delta variant,

and Omicron variant began in South Africa in May 2020, India in Oct 2020, and in multiple countries in Nov 2021 has caused worry all over the globe. The current investigations on the variant have kindled the scientists, how SARS-CoV-2 is capable to adjust and mutate with the prevailing surrounding.^[1-3] Each coronavirus includes

our structural proteins namely spike, envelope, nucleocapsid, and membrane proteins. Almost, all the mutations in the above-mentioned variants have been happening in the RBD area of the spike protein.^[4,5] These mutations will increase transmissibility^[6,7] and will increase the immune evasiveness of the virus.^[8,9] Also, it is very easy for the spike protein to mingle with the host receptors.^[10] Thus, the spike protein section is accountable for the doorway of SARS-CoV-2 in human ACE2-expressing cells. The globe is finding it difficult to overcome this pandemic situation because of these mutations which decrease the vaccine efficiency^[11] and also due to the non-availability of antiviral medicine against SARS-CoV-2.

SARS-CoV-2 spike (S) protein binds to angiotensin-converting enzyme 2 (ACE2) to gain cell entry^[12] and thus mingles with the active site of ACE2 receptor (Kd of ~15 nM).^[13] Those Cells having more expression of ACE2 may be regarded as potent SARS-CoV-2 infection sites.^[14] The occurrence of more ACE2 expression leads to an increase of more SARS-CoV-2 viral infection.^[15] COVID-19 disease may be effectively cured when we target ACE2 expression.^[16] Preventing the entry of SARS-CoV-2 into the host cell through the ACE 2 receptors may be an excellent method to antagonize COVID-19.^[17] Hence, it is essential to determine precise antagonists against ACE2 to cease SARS-CoV-2 infection. Controlling the SARS-CoV2-ACE2 binding interface may provide an excellent technique to battle against the virus.^[18] A spike glycoprotein / ACE2 binary antagonist might bind to RBD to protect the virus entry by two processes. Tiny ligands, that can influence the binding efficiency of spike protein with its receptor, could perform as the viral attachment inhibitor for infection. A literature survey revealed that 1,2,3 triazole derivatives may act as potential inhibitors against Covid - 19 proteins.^[19,20]

In the current study, three 1,2,3 triazole derivatives, namely, (*E*)-1-(1-benzyl-5-methyl-4,5-dihydro-1*H*-1,2,3-triazol-4-yl)-3-phenylprop-2-en-1-one (BMTTP), (*E*)-1-(1-benzyl-5-methyl-4,5-dihydro-1*H*-1,2,3-triazol-4-yl)-3-(*p*-tolyl)prop-2-en-1-one (BMTTP) and (*E*)-1-(1-benzyl-5-methyl-4,5-dihydro-1*H*-1,2,3-triazol-4-yl)-3-(4-isopropylphenyl)prop-2-en-1-one (BMTIP) were synthesized and their drug-likeness has been evaluated. The single crystal X-ray diffraction studies have been investigated for compound 2. For all the compounds, the optimized geometry, Homo-Lumo and Molecular electrostatic potential (MEP) has been examined by DFT procedure.

Further, in the current research work, synthesized compounds with antiviral activities, which can efficiently prevent spike protein as well as safeguard the viral binding site of ACE2 receptor protein were utilized to analyze the binary antagonists against COVID-19 by molecular docking.

2 | EXPERIMENTAL AND COMPUTATIONAL METHODS

2.1 | Synthesis procedure

A general synthesis method of the compounds BMTTP, BMTTP, and BMTIP was portrayed schematically in Scheme 1. A mixture of 1-(1-benzyl-5-methyl-4,5-dihydro-1*H*-1,2,3-triazol-4-yl)ethanone (0.1 mmol) and benzaldehyde/*p*-tolualdehyde/isopropyl benzaldehyde (**2a/2b/2c**, 0.1 mmol), were dissolved in ethanol (5 mL) with the addition of 20 mol% of NaOH and stirred for 08–15 min at ambient temperature. Once the reaction is completed (monitored by TLC), the excess crushed ice was added to the reaction mixture. The thrown-out solid product was filtered and cleaned with an excess of water to acquire triazole derivatives BMTTP, BMTTP, and BMTIP (**3a/3b/3c**).

The compound BMTTP was recrystallized with ethanol and a slow evaporation technique was utilized to get single crystals of BMTTP.

(3a) (*E*)-1-(1-benzyl-5-methyl-4,5-dihydro-1*H*-1,2,3-triazol-4-yl)-3-phenylprop-2-en-1-one

White solid, Yield: 89%; ¹H NMR (300 MHz, CDCl₃) δ: 7.99 (d, *J* = 16.0 Hz, 1H), 7.83 (d, *J* = 16.0 Hz, 1H), 7.72–7.67 (m, 2H), 7.39–7.31 (m, 3H), 7.21–7.18 (m, 3H), 7.10 (t, *J* = 8.6 Hz, 2H), 5.56 (s, 2H), 2.55 (s, 3H). ¹³C NMR (75 MHz, CDCl₃) δ: 184.13, 144.20, 142.15, 137.99, 133.92, 130.63, 130.52, 129.10, 128.58, 127.20, 122.68, 116.13, 115.84, 51.71, 9.32.

(3b) (*E*)-1-(1-benzyl-5-methyl-4,5-dihydro-1*H*-1,2,3-triazol-4-yl)-3-(*p*-tolyl)prop-2-en-1-one

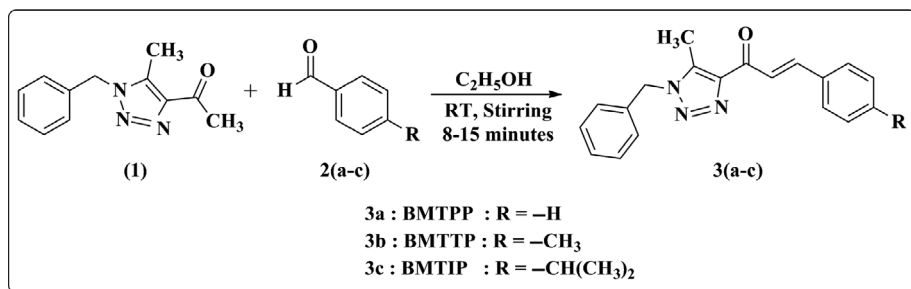
White solid, Yield: 91%; ¹H NMR (300 MHz, CDCl₃) δ: 8.02 (d, *J* = 16.0 Hz, 1H), 7.86 (d, *J* = 16.0 Hz, 1H), 7.61 (d, *J* = 8.1 Hz, 2H), 7.36–7.34 (m, 3H), 7.24–7.18 (m, 4H), 5.56 (s, 2H), 2.55 (s, 3H), 2.39 (s, 3H). ¹³C NMR (75 MHz, CDCl₃) δ: 184.34, 144.27, 143.55, 140.93, 137.83, 133.96, 132.14, 129.55, 129.03, 128.68, 128.49, 127.15, 121.89, 51.62, 21.45, 9.27.

(3c) (*E*)-1-(1-benzyl-5-methyl-4,5-dihydro-1*H*-1,2,3-triazol-4-yl)-3-(4-isopropylphenyl)prop-2-en-1-one

White solid, Yield: 90%; ¹H NMR (300 MHz, CDCl₃) δ: 8.03 (d, *J* = 16.0 Hz, 1H), 7.87 (d, *J* = 15.9 Hz, 1H), 7.65 (d, *J* = 8.2 Hz, 2H), 7.37–7.33 (m, 3H), 7.30–7.28 (m, 2H), 7.22–7.18 (m, 2H), 5.56 (s, 2H), 2.99–2.90 (m, 1H), 2.55 (s, 3H), 1.27 (d, *J* = 6.9 Hz, 6H). ¹³C NMR (75 MHz, CDCl₃) δ: 184.34, 144.27, 143.55, 140.93, 137.83, 133.96, 132.14, 129.55, 129.03, 128.68, 128.49, 127.15, 121.89, 51.62, 33.51, 21.45, 9.27.

2.2 | X-ray crystallography

Bruker APEX-II CCD with Cu-K α monochromatic radiation of wavelength $\lambda = 1.54178 \text{ \AA}$ at 296 K was utilized to



SCHEME 1 Synthesis scheme of BMTTP, BMTTP, and BMTIP

gather X-ray intensity data collection for colorless single-crystal BMTTP (size $0.15 \times 0.20 \times 0.220 \text{ mm}^3$). The X-ray diffraction data were integrated by the APEX2 (Bruker) program^[21] and SADABS^[22] was utilized to execute absorption corrections. Full-matrix least-squares refinement procedure which is based on F_o^2 was performed by the program SHELXL.^[23] The software such as WinGX^[24] and PLATON^[25] were executed to obtain crystal data and geometrical parameters for the crystal BMTTP. Mercury program^[26] was used to obtain high-quality images of the BMTTP compound and its crystal packing. The methylene H atoms are fixed in a difference Fourier map and refined isotropically. All other C-bound H atoms were placed geometrically ($C-H = 0.93-0.98 \text{ \AA}$ for sp^2 -hybridized atoms) and refined using a riding model, with $U_{iso}(H) = 1.5U_{eq}(C)$ and $1.2U_{eq}(C)$ for methyl and other H atoms, respectively.

2.3 | Computational details

2.3.1 | Density functional theory (DFT) study

DFT is an inexpensive and extensively used technique for exhibiting the ground state of molecules. The DFT procedure was performed by the most widely used functional Becke-3-Lee-Yang-Parr (B3LYP)^[27,28] method with a 6-311G(d,p) basis set,^[29] to optimize the synthesized molecules using the Gaussian03 program package.^[30] The optimized molecules are utilized to determine HOMO-LUMO, Global reactive descriptors (GRD), and Molecular Electrostatic Potential (MEP), and they were visualized using the Gauss View graphical visualization programme.^[31]

2.3.2 | Drug-likeness and ADMET computation

It is very much essential to know pharmacological and toxicity knowledge during the growth of new therapeutic drugs. This knowledge not only reduces time but also

increases the success rate of drug invention. The indices such as Absorption, Distribution, Metabolism, Excretion, and Toxicity (ADMET) are generally used to evaluate the nature of the drug. To determine these parameters, computer models are often utilized instead of experimental procedures. Molinspiration online tool^[32] (accessed on 25 February 2022) was utilized to compute drug-likeness for our synthesized compounds and Lipinski's rule of five was taken as a reference for accessing the drug-likeness.^[33] PreADMET online server^[34] (accessed on February 25, 2022) was utilized to compute the ADMET properties for our synthesized compounds.

2.3.3 | Molecular docking

In order to assess the inhibition nature and binding affinity of our synthesized compounds for curing COVID-19, a molecular docking procedure was executed with the target protein SARS-CoV-2 S-ACE2 complex (PDB ID: 7DF4) which was retrieved from the protein data bank website (<http://www1.rcsb.org>). SARS-CoV-2 S-ACE2 complex consists of a spike protein trimer and the human ACE2 receptor protein. Electron microscopy was used to solve the structure with a resolution of 3.80 \AA .^[35] Spike protein and ACE2 were detached from the complex and molecular docking analysis was carried out individually on these separated components. AutoDock Vina software and AutoDock Tools^[36] were used for Molecular docking investigations. Before molecular docking, a sequence of processes, such as preparation of protein, optimization of ligands, and selection of active site has to be completed. Water molecules and ligands were excluded from spike protein and ACE2 receptor protein with the help of the Discovery Studio 2016 visualizer program.^[37] The optimized ligands BMTTP, BMTTP, and BMTIP obtained by DFT/B3LYP/6-311G(d,p) procedure were utilized in the Docking method.

Each monomer of trimer Spike glycoprotein approximately consists of 1,261 residues.^[38] The residues 1-667 are in the S1 sub unit (N-Terminal -Domain) and the residues 668-1,261 are in the S2 sub unit (C-Terminal -

Domain). The S1 subunit is the major target for pharmaceutical researchers because it has Receptor Binding Domain (RBD) area, which is accountable for the interface of interaction with the host receptor. The residues between 319 and 541 are called as RBD area. The residues from 437 to 508 in this RBD area are called as Receptor Binding Motif (RBM) because it exactly interacts with the host's receptor. Hence, the RBD area of the spike protein was selected as an active site to dock our synthesized ligands.

With the help of AutoGrid, a grid box was formed in the active site of spike protein of 7DF4 with grid center coordinates $X = 179.351$; $Y = 187.489$; $Z = 263.305$. The contact surface of ACE2 that binds to RBD has been chosen as the best active site of ACE2 receptor protein.^[39] The important amino acids of ACE2 surface that binds with RBD area are ASP350, HIS401, PHE40, GLU375, TRP349, ASN394, LYS353, THR371, GLY326, ARG393, ARG514, and PRO399. With the help of AutoGrid, a grid box was formed in active site ACE2 receptor protein of 7DF4 with grid center coordinates $X = 171.680$; $Y = 214.638$; $Z = 285.757$. The synthesized three ligands were docked in the active site of spike protein and ACE2 receptor protein utilizing the Auto dock vina procedure. Out of the 10 different shapes obtained for each ligand-protein complex, the best-ranked complex was examined by Discovery Studio 2016 visualizer.

3 | RESULTS AND DISCUSSION

3.1 | Structural elucidation and supramolecular network

The crystal structure of compound BMTTP includes two independent molecules (A and B) in the asymmetric unit as shown in Figure 1. Details of the data collection,

crystal parameters, and refinement process of compound BMTTP are given in Table 1. The details about BMTTP crystal can be obtained in CIF form available at Cambridge Crystallographic Database centre, No. CCDC 2160301.

Figure 2 shows the overlap of non-H atoms of inverted molecule B(Blue) on molecule A (Red) with an r.m.s deviation of 1.712 Å. This high value of r.m.s deviation is due to the different orientations of the phenyl ring with respect to the triazole ring in molecule A and molecule B. In each molecule, the triazole ring is basically planar [maximum deviation = $-0.0017(18)$ Å for atom N2A of molecule A and $0.0023(19)$ Å for atom N2B of molecule B. In molecule A, the triazole ring is inclined at an angle of $83.8(1)^\circ$ and $2.30(1)^\circ$, respectively, with the phenyl (C1A-C6A) and methyl phenyl (C14A-C19A) rings, respectively, and in molecule B for the same moieties, the inclination angles are $88.9(1)^\circ$ and $5.8(1)^\circ$. The two phenyl rings are inclined at an angle of $85.7(1)^\circ$ and $88.9(1)^\circ$ in molecules A and B, respectively. In triazole rings, the bond distances and bond angles of molecules A & B are found nearer to the reported values for analogous triazole derivatives.^[40,41] The selected geometric parameters are provided in Table 2.

The two molecules are joined by an intramolecular C7B-H7B...N3A hydrogen bond. Intramolecular C10A-H10B...O1A, C13A-H13A...O1A, and C12A-H12A...N3A and hydrogen bonds in molecule A form S(6), S(5) and S(5) ring motifs, respectively. Similar intramolecular hydrogen bonds with the same ring motifs are created in molecule B. Also, an intramolecular C1B-H1B...N1B hydrogen bond in molecule B creates an S(5) ring motif. Further, a peculiar type of C-H... π interaction with C1B-H1B...Cg1 (Cg1 is the centroid of the triazole ring of molecule B) hydrogen bond is observed. These intramolecular interactions are responsible for the molecular stabilization of compound BMTTP.

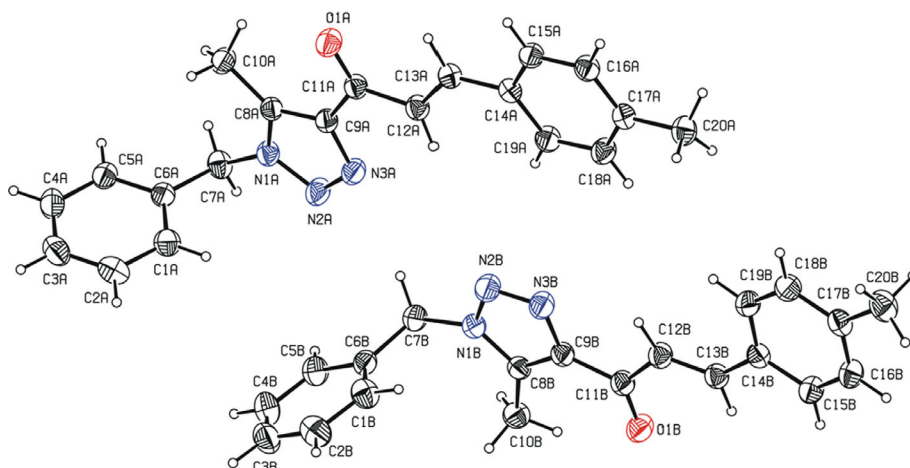


FIGURE 1 The crystal structure of compound BMTTP includes two independent molecules (A and B) in the asymmetric unit

TABLE 1 Crystal data and structure refinement parameters for BMTTP

Crystal data and parameters	BMTTP
Empirical formula	C ₄₀ H ₃₈ N ₆ O ₂
Formula weight	634.76
Temperature (K)	296(2)
Wavelength (Å)	1.54178
Crystal system	Monoclinic
Space group	P 21/c
Unit cell dimensions (Å, °)	
<i>a</i>	12.8766 (5)
<i>b</i>	14.0265 (6)
<i>c</i>	19.4155 (7)
α	90
β	100.575 (2)
γ	90
Volume (Å ³)	3,447.1 (2)
<i>Z</i>	4
Calculated density (Mg/m ³)	1.223
Absorption coefficient μ (mm ⁻¹)	0.611
F(000)	1,344
Crystal size (mm ³)	0.220 × 0.200 × 0.150
Theta range for data collection (°)	3.492–72.292
Index ranges	–15 ≤ <i>h</i> ≤ 15, –17 ≤ <i>k</i> ≤ 17, –23 ≤ <i>l</i> ≤ 23
Reflections collected	84,969
Independent reflections	6,735 [R(int) = 0.0618]
Completeness to theta	90.5%
Absorption correction	Multi-scan
Max. and min. transmission	0.914 and 0.877
Refinement method	Full-matrix least-squares on F ²
Data/restraints/parameters	6,735/0/454
Goodness-of-fit on F ²	1.039
Final R indices [I > 2σ(I)]	R1 = 0.0532, wR2 = 0.1401
R indices (all data)	R1 = 0.0658, wR2 = 0.1553
Largest diff. peak and hole (e.Å ⁻³)	0.135 and –0.130

In the crystal BMTTP, molecules are connected by three intermolecular C–H... π interactions; the first one between the methylene H atom and the phenyl ring of a nearby molecule with a C7A–H7A1...Cg2ⁱ, the second one

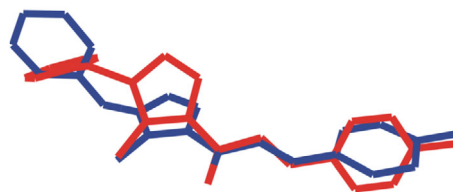


FIGURE 2 Overlap of non-H atoms of inverted molecule B (Blue) on molecule A (Red) of compound BMTTP

between phenyl H atom and phenyl ring of a nearby molecule with a C15A–H15A...Cg3ⁱⁱ and the third one between methyl H atom of the phenyl ring and phenyl ring of a nearby molecule with a C20A–H20C...Cg4ⁱⁱⁱ [Cg2, Cg3 and Cg4 are the centroids of C1A–C6A, C1B–C6B and C14B–C19B phenyl rings, respectively as shown in Figure 3. Symmetry codes: (i) $2 - x, 2 - y, 1 - z$; (ii) $x, 3/2 - y, 1/2 + z$; (iii) $-x, 1 - y, 1 - z$]. These C–H... π interactions join together to build a three-dimensional supramolecular network. The inter and intramolecular interactions observed in BMTTP are listed in Table 3.

3.2 | Optimized geometry

The optimized molecular structures for BMTTP, BMTTP, and BMTIP were portrayed in Figure 4. (DFT/B3LYP) technique along with the 6-311G(d,p) basis set was executed to obtain bond lengths, bond angles, and torsion angles for all compounds. The selected XRD geometric parameters of compound BMTTP and optimized geometric parameters of all compounds were listed in Table 2. From Table 2, it is observed that the experimental data of BMTTP matches with theoretical data for all compounds. The theoretical values of bond length and bond angle of all compounds will almost match with calculated XRD values. The XRD bond length N1–N2 (1.358(2) Å and 1.355(2) Å for molecule A & B) and N2=N3 (1.308(2) Å and 1.304(2) Å for molecule A & B) of the triazole ring in BMTTP are very well matched with DFT values for BMTTP (1.360 Å, 1.289 Å), BMTTP (1.360 Å, 1.290 Å) and BMTIP (1.364 Å, 1.290 Å). From Table 2, the experimental and theoretical bond length values of C11=O1 are almost equal. The slight variation in geometric parameters between XRD and DFT is due to the fact that experimental results are obtained in the solid phase and theoretical calculations are computed in the gas phase.

3.3 | HOMO-LUMO, GRD, and MEP analysis

The contours of the HOMO and LUMO orbitals of compounds BMTTP, BMTTP, and BMTIP by DFT/B3LYP/

TABLE 2 Selected geometry parameters of BMTTP, BMTTP, and BMTIP

Atoms	BMTTP	BMTTP		BMTIP	
	DFT	XRD		DFT	DFT
		M-A	M-B		
Bond lengths (Å)					
N1–C7	1.460	1.456(2)	1.455(2)	1.460	1.460
N1–C8	1.353	1.345(2)	1.343(2)	1.354	1.354
C8–C9	1.391	1.382(2)	1.379(2)	1.393	1.394
C11–C9	1.478	1.466(2)	1.461(2)	1.486	1.4864
C9–N3	1.368	1.362(2)	1.365(2)	1.368	1.3683
N1–N2	1.360	1.358(2)	1.355(2)	1.360	1.364
N3–N2	1.289	1.308(2)	1.304(2)	1.290	1.290
C8–C10	1.489	1.477(2)	1.478(2)	1.490	1.4905
C11–O1	1.226	1.225(2)	1.225(2)	1.229	1.229
C11–C12	1.479	1.472(2)	1.480(2)	1.473	1.474
C12–C13	1.344	1.32(2)	1.321(2)	1.347	1.347
C17–C20	—	1.503(2)	1.503(2)	1.508	1.520
C20–C21	—	—	—	—	1.539
C20–C22	—	—	—	—	1.539
Bond angles (°)					
C7–N1–C8	129.52	129.9(1)	128.8(1)	129.46	129.49
N1–C8–C9	103.46	104.1(2)	103.9(1)	103.54	103.53
N3–N2–N1	107.37	106.9(1)	107.0(1)	107.30	107.30
N2–N1–C8	111.16	111.3(1)	111.5(1)	111.26	111.25
C11–C12–C13	120.21	120.7(2)	121.2(2)	128.38	128.40
C9–C11–O1	120.78	120.1(2)	120.8(2)	118.80	118.81
O1–C11–C12	122.99	122.7(2)	122.6(2)	118.34	118.33
Torsion angles (°)					
C7–N1–C8–C10	–2.003	–0.4(3)	0.7(3)	2.138	2.227
N1–N2–N3–C9	0.038	0.3(2)	–0.4(2)	0.024	–0.002
C9–C11–C12–C13	–179.60	174.2(2)	–176.5(2)	–0.430	–0.268
C11–C12–C13–C14	–179.99	178.0(2)	–177.4(2)	179.68	179.84
O1–C11–C12–C13	0.384	–6.2(3)	4.3(3)	179.91	179.87
C15–C16–C17–C20	—	–177.7(2)	179.5(2)	–179.89	179.93
C17–C18–C19–C20	—	178.4(2)	–179.4(2)	179.92	–179.89
C16–C17–C20–C21	—	—	—	—	–63.34
C16–C17–C20–C22	—	—	—	—	62.09
C17–C18–C20–C21	—	—	—	—	116.54
C17–C18–C20–C22	—	—	—	—	–118.01

6-311G (d,p) are portrayed in Figure 5. The energy value of the uppermost filled orbital (HOMO = 6.3948, –6.2043 and –6.2032 for BMTTP, BMTTP, and BMTIP), lowermost empty orbital (LUMO = –2.1497, –2.0136 and –2.0147 and their orbital energy gap ($\Delta E = 4.2451, 4.1907$ and 4.1885

for BMTTP, BMTTP, and BMTIP) are determined and are listed in Table 4. The red and green forms denote the produced positive and negative wave functions over the compound. The HOMOs of the complex for all the compounds are spread.

mostly over the phenyl ring. The LUMOs of the complex are spread mostly over the triazole ring and oxygen atom of all the compounds and phenyl (C14–C19), methyl phenyl, and isopropyl phenyl rings in BMTTP, BMTTP, and BMTIP, respectively. The low HOMO–LUMO energy gap for all compounds describes the ultimate charge transfer that occurs within each compound and confirms the occurrence of medicinal activity for all our compounds.

The global chemical reactivity descriptor parameters such as chemical potential (μ), hardness value (η), softness (S), electronegativity (χ) and electrophilicity index (ω) (see Table 4) are obtained based on the computation of the HOMO and LUMO energy of the optimized molecule to know the relationships between the structure, stability, and reactivity of a molecule.^[42] The ionization potential (I) and electron affinity (A) of a molecule is related to the negative values of E_{HOMO} and E_{LUMO} , respectively.

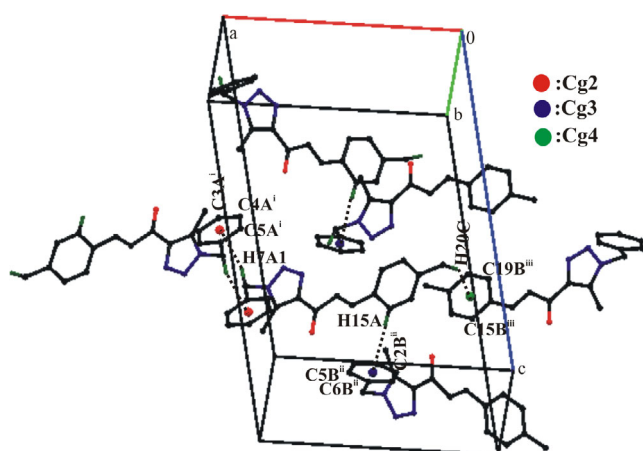


FIGURE 3 The supramolecular network of compound BMTTP

Chemical hardness (η) and softness (S) are linked with the reactivity of the molecule.^[43,44] Low η and high S values indicate that the molecule is more reactive. The η and S values listed in Table 4 confirm that our compounds are more reactive.

The large electronegativity value ($\chi = 4.2722$ eV, 4.1089 eV and 4.1089 eV for BMTTP, BMTTP, and BMTIP) indicates that our compounds are more active in catalysis.^[45] The low chemical potential value ($\mu = -4.2722$, -4.1089 and -4.1089 eV for BMTTP, BMTTP, and BMTIP) indicates that our compounds are

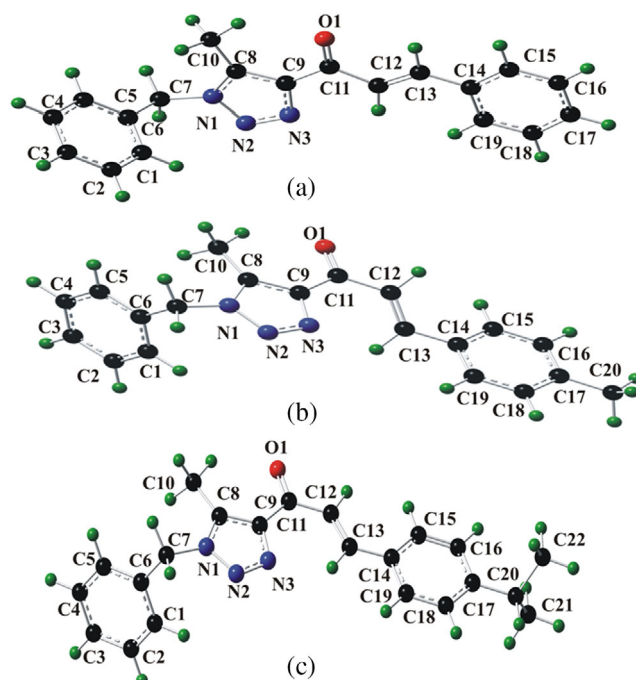


FIGURE 4 The optimized molecular structures for BMTTP, BMTTP, and BMTIP

S.no	D–H...A	D–H (Å)	H...A(Å)	D...A(Å)	D–H...A(°)
1	C7B–H7B2...N3A	0.97	2.48	3.427(3)	165
2	C1B–H1B...N1B	0.93	2.58	2.895(3)	100
3	C10A–H10B...O1A	0.96	2.57	3.116(2)	116
4	C10B–H16E...O1B	0.96	2.53	3.143(2)	121
5	C12A–H12A...N3A	0.97(2)	2.50	2.872(2)	102(1)
6	C12B–H12B...N3B	1.01(2)	2.41	2.846(2)	105.2(2)
7	C13A–H13A...O1A	0.99(2)	2.42	2.814(2)	103(1)
8	C13B–H13B...O1B	1.03(2)	2.44	2.826(2)	102(1)
9	C1B–H1B...Cg1	0.93	2.99	3.562(2)	121
10	C7A–H7A1...Cg2 ⁱ	0.97	2.70	3.610(2)	156
11	C15A–H15A...Cg3 ⁱⁱ	0.93	2.78	3.711(2)	176
12	C20A–H20C...Cg4 ⁱⁱⁱ	0.96	2.98	3.800(2)	145

TABLE 3 Inter and intra molecular interactions for BMTTP

more stable since they will retain the electron to escape from the system.^[46]

The electrophilicity (ω) index value of more than 4.00 eV are superelectrophiles indicating high reactivity in polar reactions.^[47] Table 4 shows that our compounds possess a high electrophilicity index (>4.0 eV) and in turn indicates they are highly reactive and more biologically active.

With the help of electrostatic potential distribution, molecular electrostatic potential (MEP) finds for electrophilic and nucleophilic attacks. The MEP surface is related to the electron density which explains the nucleophilic reaction and electrophilic attack and also the hydrogen bonding relations. Normally in MEP, color coding is utilized for picturing the electrostatic potential regions. Blue and red colors denote the positive and negative electrostatic potential areas, respectively, whereas green color denotes a zero potential area. As presented in

Figure 6, a large number of positive areas situated on the hydrogen atoms in the compounds BMTTP, BMTTP, and BMTIP are estimated to be promising positions for nucleophilic attack. A large number of negative areas situated on oxygen O1 and nitrogen atoms (N2 & N3) of the synthesized compounds indicated an electrophilic attack. The carbonyl oxygen atom O1 which has a greater electron density (denser red color) involves hydrogen bonding with the target implies that our synthesized compounds will have medicinal activity.

3.4 | Drug-likeness and ADMET results

The knowledge of drug-likeness offers valuable guidelines for initial stage drug discovery. Normally, the unique and most well-known Lipinski's Rule of Five (Ro5) is used as an assessment for drug-likeness. Ro5 is

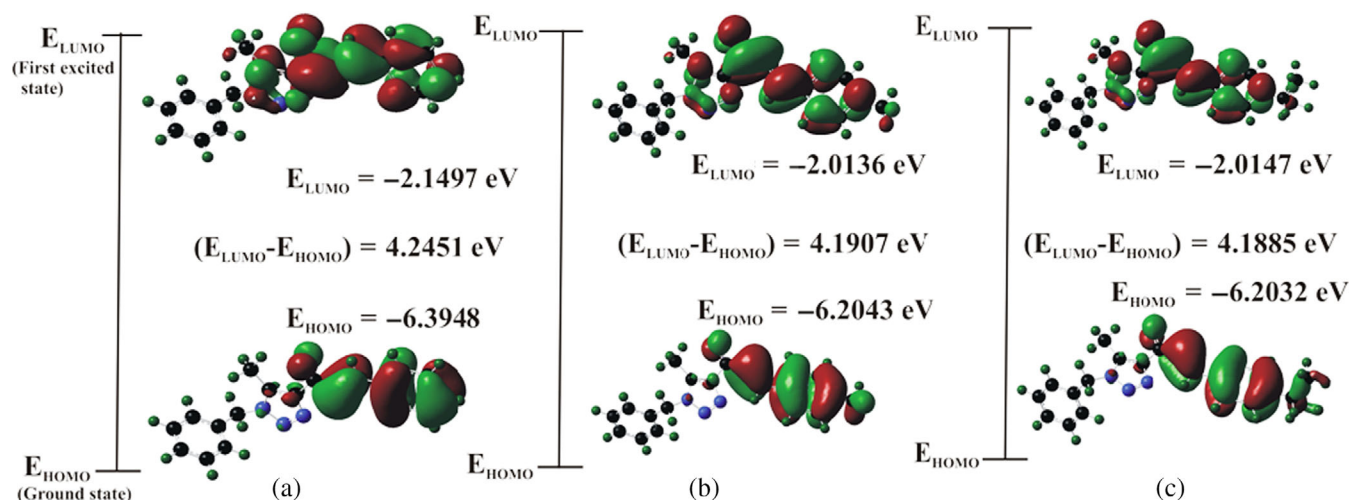


FIGURE 5 The contours of the HOMO and LUMO orbitals of compounds BMTTP, BMTTP, and BMTIP by DFT/B3LYP/6-311G(d,p)

TABLE 4 Energy of HOMO/LUMO orbitals and reactivity descriptors of BMTTP, BMTTP, and BMTIP

Parameters	BMTTP	BMTTP	BMTIP
HOMO energy (eV)	-6.3948	-6.2043	-6.2032
LUMO energy (eV)	-2.1497	-2.0136	-2.0147
$\Delta E = \text{LUMO-HOMO}$ energy gap (eV)	4.2451	4.1907	4.1885
Electron affinity (A) (eV)	2.1497	2.0136	2.0147
Ionization potential (I) (eV)	6.3948	6.2043	6.2032
Chemical hardness (η) (eV)	2.1225	2.0953	2.0942
Chemical softness (s) (eV)	0.2355	0.2386	0.2387
Chemical potential (μ) (eV)	-4.2722	-4.1089	-4.1089
Electronegativity (χ) (eV)	4.2722	4.1089	4.1089
Electrophilicity index (ω) (eV)	4.2982	4.0282	4.0299

Note: $I = -E_{\text{HOMO}}$; $A = -E_{\text{LUMO}}$; $\chi = (I + A)/2$; $\eta = (I - A)/2$; $s = 1/2\eta$; $\mu = -(I + A)/2$; $\omega = \mu^2/2\eta$.

employed to examine the oral bioavailability of the synthesized three triazole derivatives. The Lipinski's five rules are as follows: molecular weight <500 , (octanol/water coefficient) $\log p \leq 5$, hydrogen bond donors HBD ≤ 5 , hydrogen bond acceptors ≤ 10 . More than one violation in the above parameters will lead to poor absorption and permeation. The computed drug-likeness values of our compounds BMTTP, BMTTP, and BMTIP are provided in Table 5. The compound which satisfies the condition ($0 < \log p < 3$) will exhibit good oral bioavailability. The lipophilicity values of $\log P$ for our compounds BMTTP and BMTTP are less than 5 (3.78 and 2.23) indicating they are highly lipophilic, have good permeability across biological membranes, and have excellent binding to plasma proteins.^[48] Even though the $\log P$ value of compound BMTIP is slightly more than 5, the positive value suggests that it may also exhibit good oral bioavailability. The Topological polar surface area (TPSA) value of 47.79 \AA^2 for our compounds is very

much lower than 160 \AA^2 and hence our compounds are expected to behave with good oral bioavailability and transport through membranes. The other parameters such as molecular weight, hydrogen bond donors, hydrogen bond acceptors, and rotatable bonds are within the range for our synthesized compounds suggesting they could effortlessly cross cell membranes. Since all triazole derivatives satisfy the Lipinski rule of five (not more than one violation), there may be no issues in oral bioavailability.

The online computation of Absorption, Distribution, Metabolism, and Excretion (ADME) proprieties for our synthesized triazole derivatives by PreADMET online server is displayed in Table 6. The consequences of human intestinal absorption are the sum of absorption and bioavailability, assessed from the collective excretion in urine, bile, and feces.^[49,50]

The prepared ligands displayed good human intestinal absorption (HIA), having values of HIA greater than

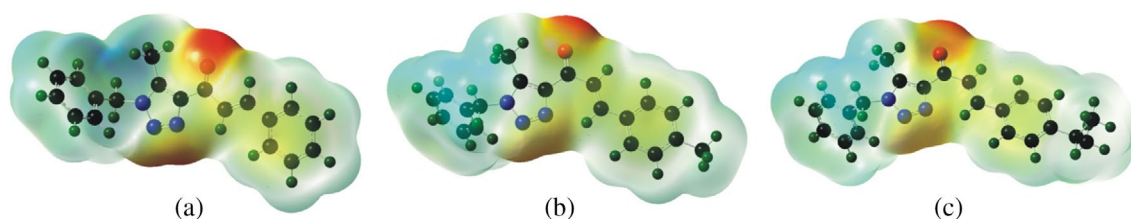


FIGURE 6 The molecular electrostatic potential (MEP) map of BMTTP, BMTTP, and BMTIP

TABLE 5 Drug-likeness values of BMTTP, BMTTP, and BMTIP by Molinspiration online server

Compounds	mi LogP ^a	TPSA ^b	MW ^c	No. of H-bond acceptors	No. of H-bond donors	No. of violation	Volume	n-atom	n-rotb ^d
BMTTP	3.78	47.79	303.37	4	0	0	283.68	23	5
BMTTP	4.23	47.79	317.39	4	0	0	300.24	24	5
BMTIP	5.29	47.79	345.45	4	0	1	333.63	26	6

^aLogarithm of partition coefficient between n-octanol and water (miLogP).

^bTopological polar surface area (TPSA).

^cMolecular weight (MW).

^dNumber of rotatable bonds (n-rotb).

TABLE 6 ADME property values of BMTTP, BMTTP, and BMTIP using the Pre ADMET online server

Compounds	Absorption			Skin permeability (logkp, cm/hour)	Distribution	
	Human intestinal absorption	CaCo-2 cell permeability (nm/s)	MDCK cell permeability (nm/s)		Plasma protein binding (%)	Blood-brain barrier penetration (c.brain/c.blood)
BMTTP	97.42	32.84	103.78	-2.49	94.73	0.3159
BMTTP	97.41	33.13	31.81	-2.44	94.30	0.0965
BMTIP	97.44	41.46	7.535	-2.20	94.27	0.1611

97.41%. CaCo-2 is a human colon epithelial cell line that is generally employed as a model system for evaluating the human intestinal assimilation of drugs. Since Madin-Darby Canine Kidney (MDCK) cells have a smaller growth period than CaCo-2 cells, MDCK cells are valuable for judging the fast permeability of drug molecule.^[51] The computed CaCo-2 cell permeability values of all our synthesized compounds were found to be in the adequate range and thus have good intestinal absorption. The MDCK cell permeability of BMTTP and BMTTP compounds were predicted high and moderate values. Hence, these two compounds are more encouraging for clearance through the kidney cells. Even though the compound BMTTP will have a low MDCK value when compared to other compounds, it may also clear through the kidney cells. The predicted negative values of skin permeability for all compounds indicate that they may not have any skin permeability effect. If the $C_{\text{Brain}}/C_{\text{Blood}}$ values of the compounds are more than 1, then, those compounds are categorized as central nervous system (CNS) active and compounds having $C_{\text{Brain}}/C_{\text{Blood}}$ values less than 1 are categorized as CNS inactive. CNS active compounds will penetrate Blood–Brain Barrier (BBB) and cause collateral effects in CNS.^[52] As evident from Table 6, the $C_{\text{Brain}}/C_{\text{Blood}}$ values of all our compounds are less than 1 and hence our compounds will not cross BBB. Therefore, our synthesized compounds are neuro-toxic free. The plasma protein binding model expressed in percentage tells us whether a compound is extremely bound to carrier proteins in the blood. The Plasma protein binding values of all our compounds are greater than 94% and

this obviously implies that our synthesized triazole derivatives exhibit good bioavailability and are not expected to be greatly bound to carrier proteins in the blood.

Investigation of toxicity is a key role in drug design which helps to recognize the harmful effects of new entities on living organisms. The online computation of toxicity indices for our synthesized triazole derivatives by *PreADMET* online server is displayed in Table 7. As evident from Table 7, all the compounds exhibit non-carcinogenicity in mouse and rat. Thus, our synthesized compounds are free from toxicity.

From the outcomes of drug-likeness and ADMET investigations, all our compounds fulfill the drug ability nature, and hence it is decided to perform in silico docking with Covid-19 spike glycoprotein and ACE2 receptor protein.

3.5 | Molecular docking results

3.5.1 | Spike protein

In order to block the entry of virus spike protein into the host's receptor, the prepared ligands BMTTP, BMTTP, and BMTIP were docked into the RBD area of the spike protein [PDB:7DF4]. We already know that the amino acids in the RBM area interact directly with the host's receptor. BMTTP-spike protein, BMTTP-spike protein, and BMTIP-spike protein complexes were built by the method of docking. Out of 10 ligand-protein docked postures [complexes] obtained by the method of docking, the best-ranked posture [based on most negative binding energy score] is selected for interpretation. The best-ranked postures were investigated by binding energies, and ligand-binding interactions. The three-dimensional picture of BMTTP-spike protein, BMTTP-spike protein and BMTIP-spike protein complexes are portrayed in Figure 7. A three-dimensional representation of the docked poses of the ligands BMTTP (Blue), BMTTP (Red) and BMTIP (Green) into the active site of the spike protein is

TABLE 7 ADME property values of BMTTP, BMTTP, and BMTIP using the Pre ADMET online server

Compounds	Carcinogenicity (mouse)	Carcinogenicity (rat)
BMTTP	Non-carcinogen	Non-carcinogen
BMTTP	Non-carcinogen	Non-carcinogen
BMTIP	Non-carcinogen	Non-carcinogen

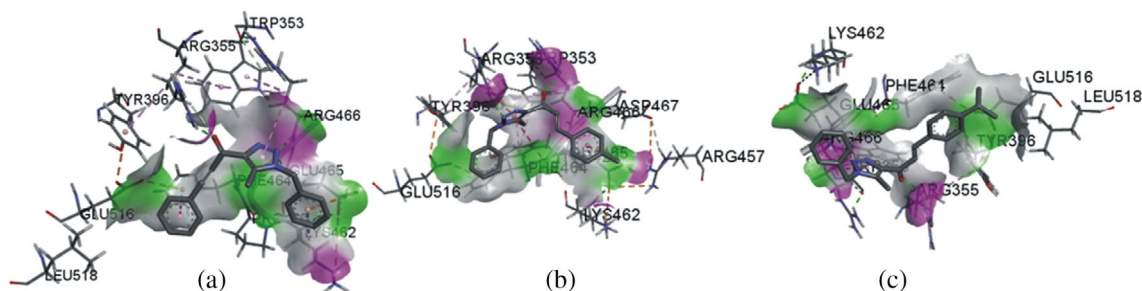


FIGURE 7 The three-dimensional picture of BMTTP-spike protein, BMTTP-spike protein, and BMTIP-spike protein docked complexes

shown in Figure 8. The different interactions in each complex are portrayed in Figure 9 and the same has been listed in Table 8.

In each docked complex, two conventional hydrogen bonds are spotted that is, the nitrogen N atom of the amino acids ARG355 and ARG466 interacts with the ligand atoms O1 and N2, respectively. Additionally, one more conventional hydrogen bond is spotted between the nitrogen N atom of the amino acid ARG466 and ligand atom N3 in BMTIP-spike protein complex. Thus, amino acid ARG466 forms a bifurcated donor hydrogen bond with ligand in BMTIP-spike protein complex. As evident from Table 8, donor-acceptor distance values of the conventional hydrogen bonds for all the three complexes are less than 4 Å. In each BMTTP-spike protein and BMTIP-spike protein complexes, one carbon-hydrogen bond is seen with carbon atom CA of the amino acid GLU465 donating its proton to atom N2 of the ligand. In each BMTTP-spike protein and BMTIP-spike protein complexes, electrostatic interaction (π -anion) is observed between the oxygen atom OE2 of the amino acid GLU465 and centroid of

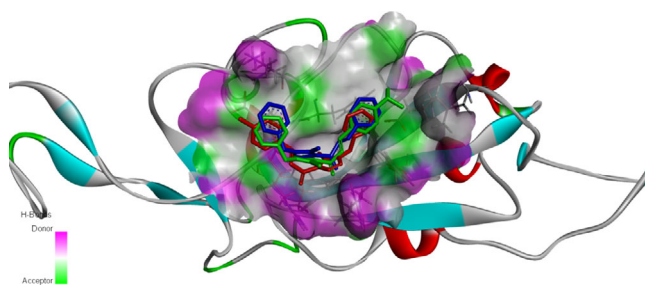


FIGURE 8 Three-dimensional representation of the docked poses of the ligands BMTTP (Blue), BMTIP (Red), and BMTIP (Green) into the active site of the spike protein (PDB code: 7DF4)

the phenyl ring (C1-C6) of the ligand. Another electrostatic interaction is spotted in BMTTP-spike protein complex between N atom of the amino acid ARG355 and centroid of the triazole ring of the ligand. Hydrophobic contacts are seen in all complexes. In each BMTTP-spike protein and BMTIP-spike protein complexes, π -sigma interaction is seen in which the carbon atom of the amino acid GLU465 interacts with the centroid of the phenyl ring (C1-C6) of the ligand through a hydrogen bond. Only in BMTTP-spike protein complex, a π - π (4.7650 Å) contact is seen between a six-membered ring of amino acid PHE464 and phenyl (C14-C19) ring of the ligand. The N atom of the amino acid PHE464 forms an amide- π (5.2834 Å) contact with the triazole ring of the ligand in BMTTP-spike protein complex. The oxygen group of the amino acid LYS462 develops a π -alkyl linkage (5.2404 Å) with the phenyl (C1-C6) ring in BMTTP-spike protein complex. Similarly, the ethylene group of the amino acid ARG466 develops a π -alkyl linkage (5.1876 Å) with the triazole ring in BMTIP-spike protein complex. Further, the outcomes of the docking investigation revealed that the synthesized ligands BMTTP, BMTIP, and BMTIP might firmly occupy the RBD area (active site) of the spike protein (PDB: 7DF4) with binding energy scores -8.9, -8.8 and -8.8 Kcal/mol, respectively.

The presence of more interactions (hydrogen bond, electrostatic and hydrophobic) and binding energy (range -8.8 to -8.9 Kcal/mol) in all ligands-spike protein complexes not only validates the stability of the docked complexes but also confirms the escalation in the medicinal activity of all our synthesized compounds. The important amino acids enclosed in the active site (RBD area) are ARG355, ARG466, GLU465, LYS462, GLU516, TRP353, TYR396, LEU518, and PHE464. Since the above amino acids are from 437 to

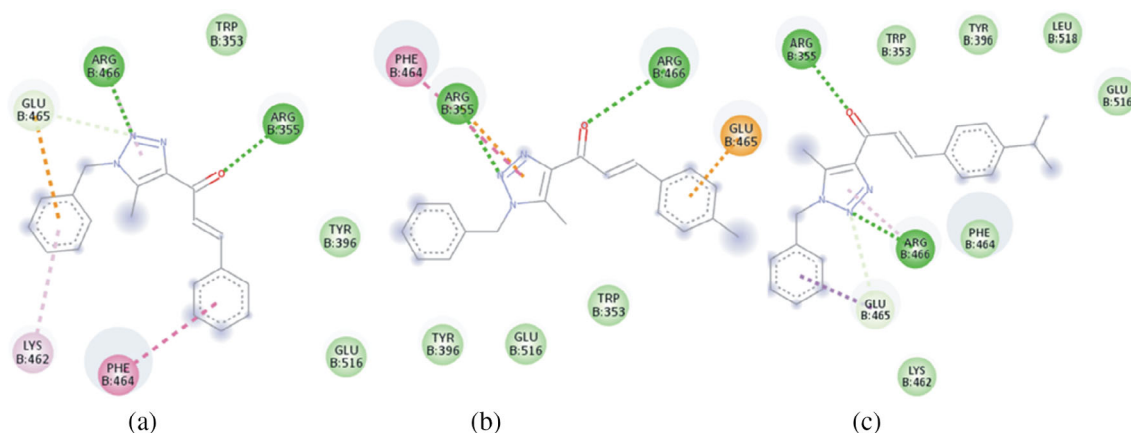


FIGURE 9 The two-dimensional docking interactions of BMTTP-spike protein, BMTIP-spike protein, and BMTIP-spike protein complexes

508, they are in the RBM area which exactly interacts with the host's receptor. Our synthesized ligands will interact with the above amino acids by way of

hydrogen, electrostatic, hydrophobic and van der Waals interactions to stop the access of the virus spike protein into the host's receptor.

TABLE 8 Binding energy, hydrogen bonds, electrostatic interactions, and hydrophobic contacts between BMTTP, BMTTP, and BMTIP ligands and Spike protein (PDB ID:7DF4)

Inhibitor	Binding energy Kcal mol ⁻¹	Interactions	Distance D...A Å	Bonding	Bonding types	Binding sites of protein	Binding sites of ligand
BMTTP	-8.9	ARG355[N-H...O1]	3.1491	Hydrogen	H-bond	N	O1
		ARG466[N-H...N2]	2.9640	Hydrogen	H-bond	N	N2
		GLU465[CA-HA...N2]	3.6828	Hydrogen	H-bond	CA	N2
		GLU465[OE2...π]	4.7341	Electrostatic	π-anion	OE2	C1-C6 phenyl ring
		PHE464[π-π]	4.7650	Hydrophobic	π-π	Six membered ring	C14-C19 phenyl ring
		[π-alkyl]LYS462	5.2404	Hydrophobic	π-alkyl	OE1	C1-C6 phenyl ring
BMTTP	-8.8	ARG355[N-H...O1]	3.9486	Hydrogen	H-bond	N	O1
		ARG466[N-H...N2]	3.2509	Hydrogen	H-bond	N	N2
		ARG355[N...π]	3.4639	Electrostatic	π-cation	N	Triazole ring
		GLU465[OE2...π]	4.5123	Electrostatic	π-anion	OE2	C1-C6 phenyl ring
		GLU465[C-H...π]	3.4713	Hydrophobic	π-sigma	C	C1-C6 phenyl ring
		PHE464[amide-π]	5.2834	Hydrophobic	Amide-π stacked	Amide	Triazole ring
BMTIP	-8.8	ARG355[N-H...O1]	3.2752	Hydrogen	H-bond	N	O1
		ARG466[N-H...N2]	2.9400	Hydrogen	H-bond	N	N2
		ARG466[N-H...N3]	3.3813	Hydrogen	H-bond	N	N3
		GLU465[CA-HA...N2]	3.7207	Hydrogen	H-bond	CA	N2
		GLU465[C-H...π]	3.8908	Hydrophobic	π-sigma	C	C1-C6 phenyl ring
		[π-alkyl]ARG466	5.1876	Hydrophobic	π-alkyl	Ethylene group	Triazole ring

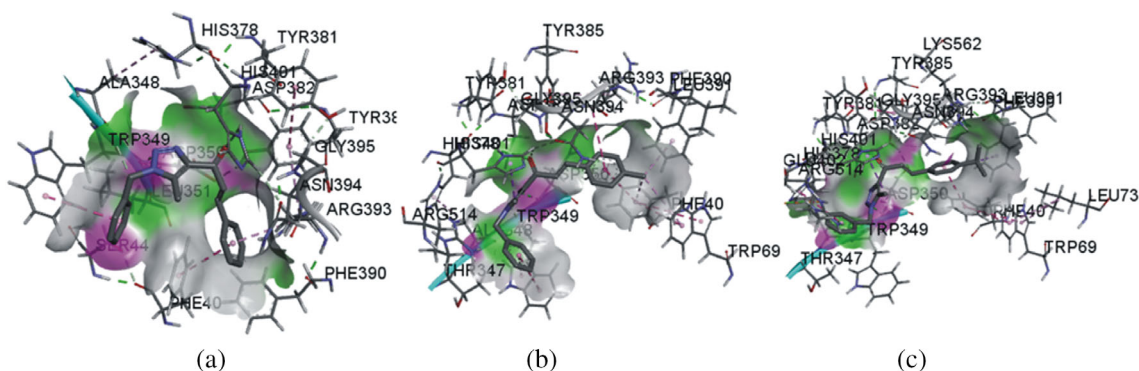


FIGURE 10 The three-dimensional picture of BMTTP-ACE2 protein, BMTTP-ACE2 protein, and BMTIP-ACE2 protein docked complexes

3.5.2 | ACE2

Till now, there are no precise ACE2 antagonists, and current ACE antagonists cannot bind to ACE2. Depending on the interface of complex 7DF4, the important amino acid residues of ACE2 antagonists were comprised of amino acid residues ASP350, HIS401, PHE40, GLU375, TRP349, ASN394, LYS353, THR371, GLY326, ARG393, ARG514, and PRO399.

BMTPP-ACE2 receptor protein, BMTPP-ACE2 receptor protein, and BMTIP-ACE2 receptor protein complexes were built by the method of docking. Out of 10 ligand-

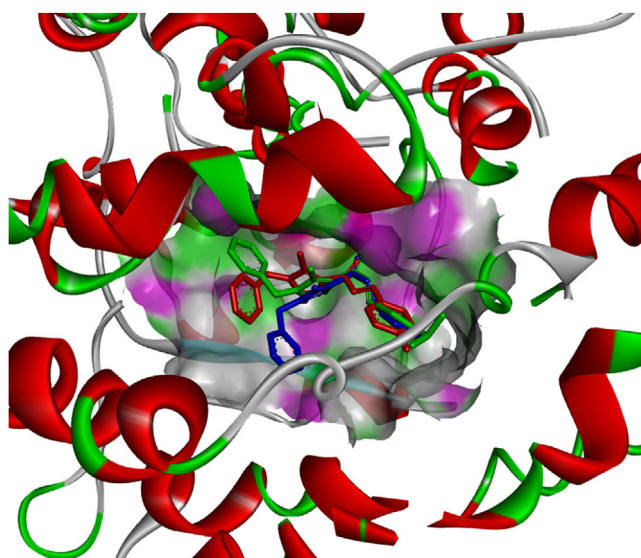


FIGURE 11 Three-dimensional representation of the docked poses of the ligands BMTPP (Blue), BMTPP (Red), and BMTIP (Green) into the active site of the ACE2 receptor protein (PDB code: 7DF4)

protein docked postures [complexes] obtained by the method of docking, the best-ranked posture [based on most negative binding energy score] is selected for interpretation. The best-ranked postures were investigated by binding energies and ligand-binding interactions. The three-dimensional picture of BMTPP-ACE2 receptor protein, BMTPP-ACE2 receptor, and BMTIP-ACE2 receptor complexes are portrayed in Figure 10. A three-dimensional representation of the docked poses of the ligands BMTPP (Blue), BMTPP (Red), and BMTIP (Green) into the active site of the ACE2 receptor protein is shown in Figure 11. The different interactions in each complex are portrayed in Figure 12 and the same has been listed in Table 9.

In each docked complex, two conventional hydrogen bonds are spotted. The nitrogen N atom of the amino acids HIS401 interacts with the ligand atoms O1 in all the docked complexes. The amino acid ASP350 interacts with the ligand atoms N2 in BMTPP-ACE2 receptor protein and BMTIP-ACE2 receptor protein complexes and ligand atom N3 in BMTPP-ACE2 receptor protein complex. As evident from Table 9, donor-acceptor distance values of the conventional hydrogen bonds for all the three complexes are less than 4 Å. One carbon-hydrogen bond is formed in BMTPP-ACE2 receptor protein complex with atom C7 of the ligand interacting with the oxygen atom of the amino acid ALA348 and two carbon-hydrogen bonds are spotted in the BMTPP-ACE2 receptor protein complex in which atom CA of TRP349 and atom CE of HIS401 interacts with ligand atoms N3 and N2, respectively. Hydrophobic contacts are seen in all complexes. In each BMTPP-ACE2 receptor protein and BMTIP-ACE2 receptor protein complex, π -sigma interaction is seen in which carbon atom C10 of the ligand interacts with the centroid of the five-membered ring of the amino acid HIS401 through a hydrogen bond. Additionally,

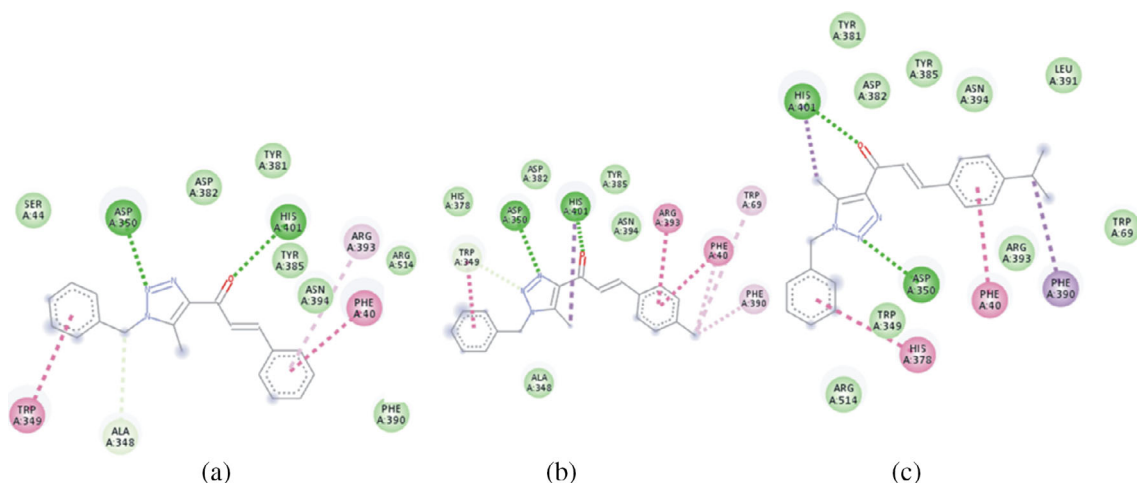


FIGURE 12 The two-dimensional docking interactions of BMTPP-ACE2 protein, BMTPP-ACE2 protein, and BMTIP-ACE2 protein complexes

TABLE 9 Binding energy, hydrogen bonds, electrostatic interactions, and hydrophobic contacts between BMTTP, BMTTP, and BMTIP ligands and ACE2 receptor protein of (PDB ID:7DF4)

Inhibitor	Binding energy Kcal mol ⁻¹	Interactions	Distance D...A Å	Bonding	Bonding types	Binding sites of protein	Binding sites of ligand
BMTTP	-9.1	HIS401[N-H... O1]	3.7078	Hydrogen	H-bond	N	O1
		ASP350[N-H... N2]	3.2401	Hydrogen	H-bond	N	N2
		[C7-H7A...O] ALA348	3.6678	Hydrogen	H-bond	O	C7
		PHE40[π - π]	4.4723	Hydrophobic	π - π	Six membered ring	C14-C19 phenyl ring
		TRP349[π - π]	4.6446	Hydrophobic	π - π	Six membered ring	C1-C6 phenyl ring
		[π -alkyl] ARG393	5.4757	Hydrophobic	π -alkyl	Ethylene group	C14-C19 phenyl ring
BMTTP	-9.1	HIS401[N-H... O1]	3.9872	Hydrogen	H-bond	N	O1
		ASP350[N-H... N3]	3.2401	Hydrogen	H-bond	N	N3
		TRP349[CA- HA...N2]	3.4145	Hydrogen	H-bond	CA	N2
		HIS401[CE- HE...O1]	3.8242	Hydrogen	H-bond	CE	O1
		[C10-H10A... π] HIS401	3.5235	Hydrophobic	π -sigma	C10	Five membered ring
		PHE40[π - π]	4.8316	Hydrophobic	π - π	Six membered ring	C14-C19 phenyl ring
		TRP349[π - π]	5.1181	Hydrophobic	π - π	Six membered ring	C1-C6 phenyl ring
		ARG393 [amide- π]	4.6732	Hydrophobic	Amide- π stacked	Amide	C14-C19 phenyl ring
		[C20- π]PHE40	4.1107	Hydrophobic	π -alkyl	Six membered ring	C20
		[C20- π]TRP69	4.7583	Hydrophobic	π -alkyl	Six membered ring	C20
[C20- π] PHE390	4.3605	Hydrophobic	π -alkyl	Six membered ring	C20		
BMTIP	-9.0	HIS401[N-H... O1]	3.6659	Hydrogen	H-bond	N	O1
		ASP350[N-H... N2]	3.4188	Hydrogen	H-bond	N	N2
		[C20-H20A... π] PHE390	3.8856	Hydrophobic	π -sigma	Six membered ring	C20
		[C10-H10A... π]	3.9357	Hydrophobic	π -sigma	Five membered ring	C10
		PHE40[π - π]	4.6948	Hydrophobic	π - π	Six membered ring	C14-C19 phenyl ring
		HIS378[π - π]	5.1114	Hydrophobic	π - π	Five membered ring	C1-C6 phenyl ring

one π - σ interaction is spotted in the BMTIP-ACE2 receptor protein complex where a carbon atom C20 of the ligand interacts with the centroid of the six-membered ring of the amino acid PHE390 through a hydrogen bond. In all the complexes a π - π (4.4723, 4.8316 and 4.6948 Å) contact is seen between the six-membered ring of amino acid PHE40 and phenyl (C14-C19) ring of the ligand. Additionally, in each BMTTP-ACE2 receptor protein and BMTTP-ACE2 receptor protein complexes, a π - π (4.6446, and 5.1181 Å) contact is seen between the six-membered ring of amino acid PHE40 and phenyl (C1-C6) ring of the ligand. Further, a π - π (5.1114 Å) contact is seen between five-membered ring of amino acid HIS378 and phenyl (C1-C6) ring of the ligand in the BMTIP-ACE2 receptor protein complex. The N atom of the amino acid ARG393 forms an amide- π (4.6732 Å) contact with the phenyl ring (C14-C19) of the ligand in BMTTP-ACE2 receptor protein complex. In the BMTTP-ACE2 receptor protein complex, the ethylene group of the amino acid ARG393 develops a π -alkyl linkage (5.4757 Å) with the phenyl (C14-C19) ring. In BMTIP-ACE2 receptor protein complex, the methyl carbon C20 forms three alkyl linkages with the six-membered ring of PHE40, TRP69, and PHE390 at distances 4.1107, 4.7583, and 4.3605 Å, respectively.

The presence of more interactions (hydrogen bond and hydrophobic) and binding energy (range -9.1 to -9.0 Kcal/mol) in all ligands-ACE2 receptor protein complexes not only confirm the stability of the docked complexes but also validates the escalation in the medicinal activity of all our synthesized compounds. The important amino acids enclosed in the active area of the ACE2 receptor are HIS401, ASP350, ARG393, PHE40, PHE390, TRP69, TRP349, ARG514, ALA348, HIS378, ASP382, TYR385, ASN394, TYR381, SER44, ARG514, LEU391. Preventing the entry of SARS-CoV-2 into the host cell through the ACE 2 receptors may be an excellent method to antagonize COVID-19. Our synthesized ligands will interact with the above amino acids by way of hydrogen, electrostatic, hydrophobic and van der Waals interactions to stop the access of the virus receptor ACE2.

Thus, the binding energy and various types of interactions obtained from the docked complexes suggest that the synthesized compounds BMTTP, BMTTP, and BMTIP may act as effective binary inhibitors against SARS-CoV-2 by simultaneously preventing the virus spike protein and virus receptor ACE2, respectively.

4 | CONCLUSIONS

The ligands BMTTP, BMTTP, and BMTIP were prepared and had been confirmed with elemental analysis. The single crystal X-ray diffraction study was performed for

the compound BMTTP. A 3D supramolecular network is achieved by three intermolecular C-H... π interactions for the ligand BMTTP. Optimized geometric parameters for all the synthesized compounds were attained by the DFT procedure. Homo-Lumo, MEP, and Global reactive descriptor investigations obtained by the DFT procedure confirm that the synthesized compounds reveal medicinal activity. Investigations of the drug-likeness and ADMET indices for our prepared ligands (BMTTP, BMTTP, and BMTIP) have revealed that these ligands have good oral drug-like properties and are free from toxicity and hence they may be considered as good oral drug candidates. Molecular docking investigations of the three synthesized ligands were performed individually into the active sites of spike protein and ACE2 receptor protein of model SARS-CoV-2. The higher binding energy and various types of interactions obtained from the docked complexes suggest that the prepared ligands BMTTP, BMTTP, and BMTIP may act as effective binary inhibitors against SARS-CoV-2 by simultaneously preventing the virus spike protein and virus receptor ACE2, respectively. In the future, we will perform molecular simulation studies followed by in vivo assay studies for our synthesized compounds. Further, the current research work will motivate the research community to prepare novel triazole derivatives to inhibit the deadly SARS-CoV-2 virus.

AUTHORS CONTRIBUTION

Saminathan Murugavel: Conceptualization, Methodology, Software, Validation, Supervision, Investigation, Writing - original draft, Writing-Review and editing. **Perumal Vasudevan:** Writing -original draft, Visualization, Investigation. **RaviKumar Chandrasekaran:** Data curation, Visualization, Software, Validation. **Vellingiri Archana:** Formal analysis, Resources. **Alagusundaram Ponnuswany:** Formal analysis, Resources.

ACKNOWLEDGMENT

The authors thank Dr. P.K. Sudhadevi Antharjanam, SAIF, IIT Madras, Chennai, India for her help with the SCXRD measurements.

FUNDING INFORMATION

This work was supported by the Tamil Nadu State Council for Science and Technology, DOTE Campus, Chennai, Tamil Nadu, India [Grant No. TNSCST/STP/PS-03/2019-20/3680 March 29, 2021].

CONFLICT OF INTEREST

The authors declare that they have no known competing financial interests or personal relationships that could have appeared to influence the work reported in this paper.

ORCID

Saminathan Murugavel  <https://orcid.org/0000-0002-4626-8104>

RaviKumar Chandrasekaran  <https://orcid.org/0000-0001-6981-5142>

REFERENCES

- [1] M. Salvatore, R. Bhattacharyya, S. Purkayastha, L. Zimmermann, D. Ray, A. Hazra, M. Kleinsasser, T. Mellan, C. Whittaker, S. Flaxman, S. Bhatt, S. Mishra, B. Mukherjee, *MedRxiv* **2021**, 06.23.21259405. <https://doi.org/10.1101/2021.06.23.21259405>.
- [2] M. N. Uddin, S. Begum, J. Akter, S. S. Ahmed, M. D. S. Rahman, W. Shumi, *J. Chin. Chem. Soc.* **2022**, 69(4), 703. <https://doi.org/10.1002/jccs.202100319>.
- [3] A. S. M. Al-Janabi, A. M. Saleh, M. R. Hatshan, *J. Chin. Chem. Soc.* **2021**, 68(6), 1104. <https://doi.org/10.1002/jccs.202000504>.
- [4] Y. Shu, J. McCauley, *Euro. Surveill.* **2017**, 22, 3.
- [5] J. Khateeb, Y. Li, H. Zhang, *Crit. Care* **2021**, 25, 244.
- [6] L. Zhang, C. B. Jackson, H. Mou, A. Ojha, H. Peng, B. D. Quinlan, E. S. Rangarajan, A. Pan, A. Vanderheiden, M. S. Suthar, W. Li, T. Izard, C. Rader, M. Farzan, H. Choe, *Nat. Commun.* **2020**, 11, 6013.
- [7] E. Volz, V. Hill, T. John, et al., *Cell* **2021**, 184(1), 64.
- [8] Y. Weisblum, F. Schmidt, F. Zhang, J. DaSilva, D. Poston, J. C. C. Lorenzi, F. Muecksch, M. Rutkowska, H. H. Hoffmann, E. Michailidis, C. Gaebler, M. Agudelo, A. Cho, Z. Wang, A. Gazumyan, M. Cipolla, L. Luchsinger, C. D. Hillyer, M. Caskey, D. F. Robbiano, C. M. Rice, M. C. Nussenzweig, T. Hatziioannou, P. D. Bieniasz, *bioRxiv* **2020**, 07.21.214759. <https://doi.org/10.1101/2020.07.21.214759>.
- [9] J. Verma, N. Subbarao, *Virology* **2021**, 561, 107.
- [10] N. Teruel, O. Mailhot, R. J. Najmanovich, *PLoS Comput. Biol.* **2021**, 17(8), e1009286. <https://doi.org/10.1371/journal.pcbi.1009286>.
- [11] J. Y. Noh, H. W. Jeong, E. C. Shin, *Sig. Transduct. Target Ther.* **2021**, 6, 203.
- [12] M. Hoffmann, H. Kleine-Weber, N. Krüger, M. Müller, C. Drosten, S. Pöhlmann, *bioRxiv* **2020**, 184, 64.
- [13] D. Wrapp, N. Wang, K. S. Corbett, J. A. Goldsmith, C.-L. Hsieh, O. Abiona, B. S. Graham, J. S. McLellan, *Science* **2020**, 367(6483), 1260.
- [14] C.-Y. Wu, Y.-S. Lin, Y.-H. Yang, L.-H. Shu, Y.-C. Cheng, H. T. Liu, *Biomed. Pharmacother.* **2020**, 132, 110816.
- [15] X. Ou, Y. Liu, X. Lei, P. Li, D. Mi, L. Ren, L. Guo, R. Guo, T. Chen, J. Hu, Z. Xiang, Z. Mu, X. Chen, J. Chen, K. Hu, Q. Jin, J. Wang, Z. Qian, *Nat. Commun.* **2020**, 11, 1620.
- [16] S. Swaminathan, M. Dehghan, J. M. Raj, T. Thomas, S. Yusuf, *BMJ* **2021**, 372, m4948. <https://doi.org/10.1136/bmj.m4948>.
- [17] D. Lu, S. Chatterjee, K. Xiao, I. Riedel, Y. Wang, R. Foo, C. Bär, T. Thum, *J. Mol. Cell. Cardiol.* **2020**, 148, 46.
- [18] S. Sharifkashani, M. A. Bafrani, A. S. Khaboushan, M. Pirzadeh, A. Kheirandish, H. Yavarpour_Bali, et al., *Eur. J. Pharmacol.* **2020**, 884, 173455. <https://doi.org/10.1016/j.ejphar.2020.173455>.
- [19] M. R. Aouad, D. J. O. Khan, M. A. Said, N. S. Al-Kaff, N. Rezki, A. A. Ali, N. Bouqellah, *Chem. Select.* **2021**, 6(14), 3468.
- [20] M. A. Said, D. J. O. Khan, F. F. Al-Blewi, N. S. Al-Blewi, A. A. Ali, N. Rezki, M. R. Aouad, M. Hagar, *Vaccines* **2021**, 9(9), 1012.
- [21] A.X.S. Bruker, Inc, *Apex 2. Bruker advanced X-ray solutions*, Madison, Wisconsin, Bruker AXS, Inc; **2004**, 53711.
- [22] G.M. Sheldrick, SADABS, Version 2.10, University of Göttingen, Germany, **2003**.
- [23] G. M. Sheldrick, *Acta Crystallogr. Sect. C Struct. Chem.* **2015**, 71(1), 3.
- [24] L. J. Farrugia, *J. Appl. Crystallogr.* **1999**, 32(4), 837.
- [25] A. L. Spek, *Acta Crystallogr. Sect. A Found. Crystallogr.* **1990**, 46(s1), c34.
- [26] C. F. Macrae, P. R. Edgington, P. McCabe, E. Pidcock, G. P. Shields, R. Taylor, J. V. D. Streek, *J. Appl. Crystallogr.* **2006**, 39(3), 453.
- [27] A. D. Becke, *J. Chem. Phys.* **1993**, 98, 5648.
- [28] C. Lee, W. Yang, R. G. Parr, *Phys. Rev. B* **1988**, 37, 785.
- [29] R. Ditchfield, W. J. Hehre, J. A. Pople, *J. Chem. Phys.* **1971**, 54, 724.
- [30] M. J. Frisch, G. W. Trucks, H. B. Schlegel, G. E. Scuseria, M. A. Robb, J. R. Cheeseman, J. A. Montgomery, T. Vreven Jr., K. N. Kudin, J. C. Burant, J. M. Millam, S. S. Iyengar, J. Tomasi, V. Barone, B. Mennucci, M. Cossi, G. Scalmani, N. Rega, G. A. Petersson, H. Nakatsuji, M. Hada, M. Ehara, K. Toyota, R. Fukuda, J. Hasegawa, M. Ishida, T. Nakajima, Y. Honda, O. Kitao, H. Nakai, M. Klene, X. Li, J. E. Knox, H. P. Hratchian, J. B. Cross, C. Adamo, J. Jaramillo, R. Gomperts, R. E. Stratmann, O. Yazyev, A. J. Austin, R. Cammi, C. Pomelli, J. W. Ochterski, P. Y. Ayala, K. Morokuma, G. A. Voth, P. Salvador, J. J. Dannenberg, V. G. Zakrzewski, S. Dapprich, A. D. Daniels, M. C. Strain, O. Farkas, D. K. Malick, A. D. Rabuck, K. Raghavachari, J. B. Foresman, J. V. Ortiz, Q. Cui, A. G. Baboul, S. Clifford, J. Cioslowski, B. B. Stefanov, G. Liu, A. Liashenko, P. Piskorz, I. Komaromi, R. L. Martin, D. J. Fox, T. Keith, M. A. Al-Laham, C. Y. Peng, A. Nanayakkara, M. Challacombe, P. M. W. Gill, B. Johnson, W. Chen, M. W. Wong, C. Gonzalez, J. A. Pople, *Gaussian03*, Gaussian Inc., Wallingford, CT, USA **2004**.
- [31] R. Dennington II, T. Keith, J. Millam, *GaussView*, Version 4.1.2, Semichem Inc., Shawnee Mission, KS, **2007**.
- [32] Molinspiration Cheminformatics free web services, <https://www.molinspiration.com>, Slovensky Grob, Slovakia. (Accessed on 25 February 2022)
- [33] C. A. Lipinski, F. Lombardo, B. W. Dominy, P. J. Feeney, *Adv. Drug Deliv. Rev.* **2012**, 64, 4.
- [34] S. K. Lee, G. S. Chang, I. H. Lee, J. E. Chung, K. Y. Sung, K. T. No, *EuroQSAR* **2004**, 9, 5 PreADMET web-based application, <https://preadmet.bmdrc.kr/> (Accessed on 25 February 2022).
- [35] C. Xu, Y. Wang, C. Liu, C. Zhang, W. Han, X. Hong, et al., *bioRxiv* **2020**, 06.30.177097. <https://doi.org/10.1101/2020.06.30.177097>.
- [36] O. Trott, A. J. Olson, *J. Comput. Chem.* **2010**, 31, 455.
- [37] D. S. Biovia, *Biovia discovery studio visualizer, v16.1.0*, Dassault - Systemes, San Diego, Dassault Systèmes; **2016**.
- [38] J. A. Jaimes, N. M. André, J. S. Chappie, J. K. Millet, G. R. Whittaker, *J. Mol. Biol.* **2020**, 432, 3309.
- [39] E. Mamidala, R. Davella, M. P. Kumar, et al., *Saudi J. Biol. Sci.* **2022**, 29(2), 840.
- [40] J. H. Malarkodi, S. Murugavel, J. E. Rosaline, M. Dinesh, A. Ponnuswamy, *Braz. J. Phys.* **2019**, 49(1), 28.
- [41] J. H. Malarkodi, S. Murugavel, J. E. Rosaline, M. Dinesh, A. Ponnuswamy, *J. Chin. Chem. Soc.* **2019**, 66(2), 205.

- [42] P. K. Chattaraj, R. Vijayaraj, V. Subramanian, *J. Chem. Theory Comput.* **2009**, *5*, 2744.
- [43] R. G. Parr, R. G. Pearson, *J. Am. Chem. Soc.* **1983**, *105*, 7512.
- [44] R. G. Pearson, *J. Chem. Sci.* **2005**, *117*, 369.
- [45] N. V. Tzouras, S. P. Neofotistos, G. C. Vougioukalakis, *ACS Omega* **2019**, *4*, 10279.
- [46] P. K. Chattaraj, S. Nath, B. Maiti, Reactivity descriptors. in *Computational medicinal chemistry for drug discovery* (Eds: B. Patrick, D. W. Hans, L. Wilfried, P. T. Jan), Marcel Dekker, New York, NY **2004**.
- [47] Y. P. Semenyuk, P. G. Morozov, O. N. Burov, M. K. Kletskii, A. V. Lisovin, S. V. Kurbatov, F. Terrier, *Tetrahedron* **2016**, *72*, 2254.
- [48] P. Ertl, B. Rhode, P. Selzer, *J. Med. Chem.* **2020**, *43*(20), 3714.
- [49] Y. H. Zhao, J. Le, M. H. Abraham, A. Hersey, P. J. Eddershaw, C. N. Luscombe, D. Butina, G. Beck, B. Sherborne, I. Cooper, *J. Pharm. Sci.* **2001**, *90*, 749.
- [50] S. Yamashita, T. Furubayashi, M. Kataoka, T. Sakane, H. Sezaki, H. Tokuda, *Eur. J. Pharm.* **2000**, *10*, 195.
- [51] M. R. Rodić, V. M. Leovac, L. S. Jovanović, V. Spasojević, M. D. Joksović, T. Stanojković, *Europ. J. Med. Chem.* **2016**, *115*, 75.
- [52] G. W. Ajay, M. A. Bemis, *J. Med. Chem.* **1999**, *42*, 4942.

SUPPORTING INFORMATION

Additional supporting information may be found in the online version of the article at the publisher's website.

How to cite this article: S. Murugavel, P. Vasudevan, R. Chandrasekaran, V. Archana, A. Ponnuswany, *J. Chin. Chem. Soc.* **2022**, *69*(6), 884.
<https://doi.org/10.1002/jccs.202200140>